

## Optical generation of terahertz and second-harmonic light in plasma-activated silicon nanophotonic structures

M. Wächter,<sup>1</sup> C. Matheisen,<sup>1</sup> M. Waldow,<sup>1</sup> T. Wahlbrink,<sup>2</sup> J. Bolten,<sup>2</sup> M. Nagel,<sup>1,a)</sup> and H. Kurz<sup>1,2</sup>

<sup>1</sup>*Institute of Semiconductor Electronics, RWTH Aachen University, Sommerfeldstraße 24, 52074 Aachen, Germany*

<sup>2</sup>*AMO GmbH, Otto-Blumenthal-Straße 25, 52074 Aachen, Germany*

(Received 26 July 2010; accepted 25 September 2010; published online 20 October 2010)

Plasma-activated silicon structures exhibit symmetry broken surfaces through chemical surface modification leading to a considerable second-order nonlinear optical response. This nonlinear response is demonstrated in second-harmonic and difference frequency generation measurements including the generation of terahertz radiation in silicon photonic nanowires using telecom wavelength excitation pulses. © 2010 American Institute of Physics. [doi:10.1063/1.3503586]

Previous efforts or proposals aiming at the realization of silicon photonic structures with second-order nonlinearity were based on cladding the silicon waveguide with an additional (predominantly organic) electro-optic material.<sup>1,2</sup> However, fabrication including the process step of electric field-induced poling of the applied polymer material—is complex and difficult to integrate into complementary metal-oxide-semiconductor (CMOS) production lines. Silicon itself exhibits a second-order dipole response at the surface, where the bulk inversion symmetry is broken.<sup>3</sup> Electric fields (e.g., in the space-charge region) generate an additional anisotropy within the biased volume,<sup>4</sup> which has been optically studied by electric-field-induced second-harmonic generation (SHG).<sup>5</sup> Alternatively, mechanical strain generated by the deposition of highly braced cladding layers<sup>6</sup> has also been used for anisotropy generation in silicon. However, the implementation and local application of such silicon-intern approaches into nanophotonic devices is still difficult and hence the number of experimental demonstrations published to date is very sparse. In this work a novel approach based on a simple CMOS-compatible plasma process is demonstrated to induce enhanced second-order nonlinearity at silicon surfaces. This enhancement, which is caused by a plasma-assisted chemical surface treatment, is verified in two independent experiments: SHG and difference frequency generation (DFG), e.g. terahertz (THz) generation.

The fabrication of the plasma-activated (PA) silicon structures starts from silicon-on-insulator (SOI) material commercially available from S.O.I.TEC, France. The SOI-layer system contains a 625  $\mu\text{m}$  thick handle wafer with a phosphorous background doping resulting in a specific resistivity of  $<2 \Omega \text{ cm}$ . The handle layer is covered by a 2  $\mu\text{m}$  thick buried oxide layer followed by a 340 nm thick silicon layer on top with  $\langle 100 \rangle$  orientation and the same background doping and specific resistivity as the handle wafer. First, the top silicon layer is thinned to a thickness of 220 nm (88 nm for SHG measurements) by thermal oxidization and subsequent removal of silicon dioxide in hydrofluoric acid. The resulting structure is used as a reference slab-waveguide (SWG). Plasma-activated SWGs are obtained by adding a short exposure of the sample to an HBr-plasma [gas flow: 50

SCCM (SCCM denotes cubic centimeter per minute at STP), pressure: 5 mtorr] for about three seconds as a final process step. Reactive ion etching (RIE) in an HBr-plasma is a standard CMOS-process often used for anisotropic etching of silicon. During the process Bromine chemisorbs on the Si surface in a reaction layer which is typically only one monolayer thick. After the short etching process ionic Si-Br<sub>x</sub> bonds ( $1 \leq x \leq 3$ ) are left at the surface. This is expected to result in a charge center dislocation and consequently in a break of centrosymmetry in the vicinity of the silicon surface. As verified by atomic force microscopy the short RIE etching process step removes less than 4 nm of silicon. A significant modification of surface roughness is not observed. For SHG measurements an additional set of PA and reference samples are prepared using the described processes and  $\langle 100 \rangle$ - and  $\langle 111 \rangle$ -oriented bulk silicon material.

First, the second-order optical nonlinearity of the prepared surfaces is investigated by rotational anisotropic SHG.<sup>3</sup> The second-harmonic of an incident optical beam is dominantly generated at the surface of the silicon crystal, where the bulk centrosymmetry is broken. However, since the layer of second-order activity at the surface is usually very thin, bulk quadrupolar contributions  $\chi_{\text{bulk}}^{(2)Q}$  are often not negligible. Strain or static electric fields  $E_{\text{dc}}$  contribute to the effective nonlinear polarization  $P_{\text{NL}}$  as well. The total second harmonic polarization can be expressed as

$$P_{\text{NL}}(2\omega) = \varepsilon_0 [\chi_{\text{bulk}}^{(3)} E(\omega) E(\omega) E_{\text{dc}} + \chi_{\text{surf}}^{(2)} E(\omega) E(\omega) + \chi_{\text{bulk}}^{(2)Q} E(\omega) \nabla E(\omega)], \quad (1)$$

where  $\chi_{\text{surf}}^{(2)}$  describes the surface contribution of the second order nonlinearity and  $E(\omega)$  represents the electrical field of the incident light. The resulting intensity  $I_{\text{SHG}}$  of the second harmonic light from a silicon surface can be described as a function of the azimuthal angle  $\varphi$  with respect to crystalline surface orientation by

$$I_{\text{SHG},xy} = |a_{xy} + b_{xy} \cos(3\varphi)|^2 I_x^2, \quad (2)$$

for a  $\langle 111 \rangle$ -oriented surface and

$$I_{\text{SHG},xy} = |a_{xy} + b_{xy} \cos(4\varphi)|^2 I_x^2, \quad (3)$$

for a  $\langle 100 \rangle$ -oriented surface, where the indices  $x, y \in \{s, p\}$  indicate the considered incident fundamental and detected

<sup>a)</sup>Electronic mail: nagel@iht.rwth-aachen.de.

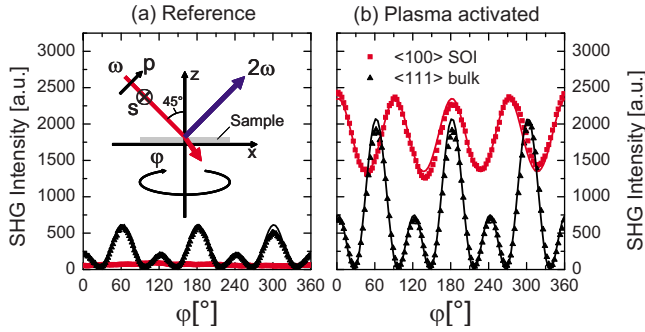


FIG. 1. (Color online) Measured and fitted SH intensity data vs azimuthal angle of the incident plane for (a) the reference and (b) the plasma-activated samples, for both figures measured at the surface of  $\langle 111 \rangle$  bulk material and of an  $\langle 100 \rangle$  SOI structure with a 88-nm-thick top silicon layer. Also in (a): schematic description of the applied RASHG measurement configuration.

SHG polarizations. The isotropic and anisotropic coefficients  $a_{xy}$  and  $b_{xy}$ , respectively, include the Fresnel coefficient and the contributions of the nonlinear optic tensor components. The experimental configuration used for the SHG experiments is schematically depicted in the inset diagram of Fig. 1(a). Laser pulses at a center wavelength  $\lambda=810$  nm (1.53 eV), a repetition rate  $f_{\text{rep}}=80$  MHz and a pulse duration of  $\tau_{\text{FWHM}}=120$  fs are used for excitation. The pulse train is directed on the sample surface at an incident angle of  $45^\circ$  with an average power of 130 mW. The reflected SH light (3.06 eV) is isolated from the fundamental beam using a Pellin–Broca prism and spectral filters and is quantified with a single photon counter based on a photomultiplier.

Exemplary experimental and theoretical fit data are plotted in Fig. 1. For all samples, a significant second-order nonlinearity enhancement is observed at the PA surfaces in comparison to the reference surfaces. The susceptibility enhancements are summarized in Table I. Most values measured at the PA bulk samples are of comparable size or partly even higher than strain-induced values (1.6–2.55), recently measured at bulk surfaces for stress values in the GPa-range.<sup>7</sup> A surprisingly high susceptibility enhancement  $b_{sp}^{\text{enh}}$ , however, is observed at the SOI sample. Unfortunately, since the corresponding fourfold SHG contribution from the reference sample was below the noise limit of our measurement set-up we can only specify a minimum value for this enhancement factor, which is given by  $b_{sp}^{\text{enh}} > 24$ . The actual value is even larger. The considerably increased enhancement observed at the SOI sample in comparison to the bulk sample can be explained by interference-induced field enhancement within the top silicon layer.<sup>8</sup>

TABLE I. Comparison of plasma-induced susceptibility enhancements at investigated samples.

Sample $E_{\text{SHG}}=3.06$ eV	Azimuthal SHG signal	Plasma-induced susceptibility enhancement	Strain-induced susceptibility enhancement
$\langle 111 \rangle$ Bulk	$I_{ps} =  a_{ps} + b_{ps} \cos(3\varphi) ^2 I_0^2$ $I_{ss} =  b_{ss} \cos(3\varphi) ^2 I_0^2$ $I_{pp} =  a_{pp} + c_{pp} \cos(3\varphi) ^2 I_0^2$	$b_{ps}^{\text{enh}} = 2.0$ $b_{ss}^{\text{enh}} = 1.8$ $a_{pp}^{\text{enh}} = 1.5, b_{pp}^{\text{enh}} = 1.9$	$a_{pp}^{\text{enh}} = 2.55, b_{pp}^{\text{enh}} = 1.6, E_{\text{SHG}} = 3.1 \text{ eV}^a$
$\langle 100 \rangle$ Bulk	$I_{sp} =  a_{sp} + b_{sp} \cos(4\varphi) ^2 I_0^2$	$a_{sp}^{\text{enh}} = 2.5, b_{sp}^{\text{enh}} = 3.4$	$b_{sp}^{\text{enh}} = 1.9, E_{\text{SHG}} = 3.26 \text{ eV}^a$
$\langle 100 \rangle$ SOI	$I_{sp} =  a_{sp} + b_{sp} \cos(4\varphi) ^2 I_0^2$	$a_{sp}^{\text{enh}} = 5.4, b_{sp}^{\text{enh}} > 24$	

<sup>a</sup>Data from Ref. 7.

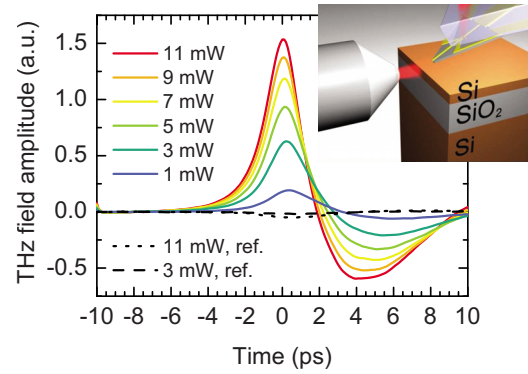


FIG. 2. (Color online) Experimental time-domain data of terahertz field signals  $E_z(t)$  generated for different optical excitation power at the PA and reference silicon slab waveguides ( $h=220$  nm). Upper right picture: Schematic of the experimental configuration used for THz signal generation.

Next, terahertz signal generation via DFG is investigated. In contrast to our previous experiments, the second-order nonlinear process is now pumped below the energy band-gap of silicon and the excitation signal is transmitted through the SWG. The experimental configuration is sketched in the upper right inlay in Fig. 2. The setup is based on a classic optical pump/probe scheme. Broadband pulses with a center wavelength  $\lambda=1550$  nm, duration  $\tau_{\text{FWHM}}=100$  fs and repetition rate  $f_{\text{rep}}=100$  MHz are split into a pump and a probe beam. The TM-polarized pump beam is coupled into the silicon waveguide using a single-mode polarization maintaining lensed fiber. The coupling loss is approx. 20 dB. Hence, from 11 mW of average power at the fiber output only  $110 \mu\text{W}$  are coupled into the silicon waveguide and the corresponding maximum pulse peak power within the waveguide is 10 W. Unless otherwise stated, all power values referred to in this paper are fiber output values. The generated THz signals are detected with a freely-positionable photoconductive (PC) probe-tip held in slight contact to the silicon surface. With this tip (similar to the one described in Ref. 9) the  $E_z$ -field component at the silicon surface can be detected with a spatial resolution better than  $5 \mu\text{m}$  and subpicosecond time resolution. The detector is equipped with a fast photoswitch based on low-temperature-grown gallium-arsenide (LT-GaAs), which is sampled by the delayed probe pulses for time-resolved field detection.

Terahertz signals from both SWGs are plotted in Fig. 2. The lateral distance between the in-coupling facet and the field probing position is  $100 \mu\text{m}$ . A 64-times higher peak amplitude is observed at the PA SWG for 1 mW average excitation power. At the PA (reference) waveguide the de-

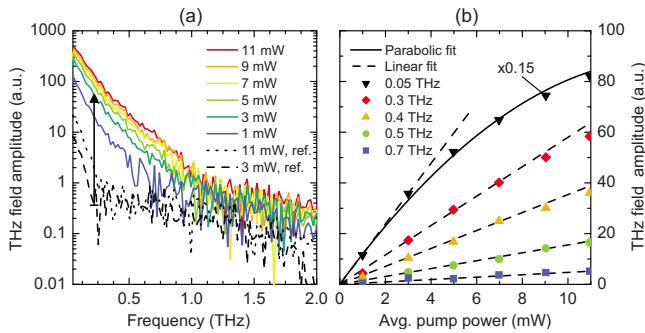


FIG. 3. (Color online) (a) Frequency-domain data of the THz amplitudes generated at the PA and reference slab waveguide as a function of varying optical excitation power. (b) Terahertz frequency-domain field amplitudes plotted against average pump power. Field amplitudes for  $f=0.005$  THz are multiplied by 0.25 for better visualization.

tected time-domain signals exhibit an initial positive (negative) pulse followed by a half-cycle in the negative (positive) amplitude range, respectively. The postpulse half-cycle is generated by probe internal reflection. For increasing excitation power the generated THz field amplitude increases and the full-width-half-maximum (FWHM) duration of the pulses decreases from 2.6 ps to 1.7 ps for an excitation power increasing from 1 mW to 40 mW, respectively. Remarkably, pulse reshaping is not observed at the non-activated reference waveguide. The reference SWG pulse duration is also much longer (4.2 ps, FWHM) than the pulse durations measured at the PA SWG. In standard Si photonic waveguides two-photon absorption and self-phase modulation have been identified as the dominating (third-order) nonlinear effects responsible for significant pulse spectrum broadening and saturation of transmission power for peak intensities above  $\sim 0.05$  GW/cm<sup>2</sup>.<sup>10</sup> The maximum waveguide-internal peak intensity in our study is estimated to be approximately around this characteristic limit. A full theoretical description of the underlying short-pulse dispersion effects in PA silicon waveguides will require an extension of existing models, which are so far solely based on linear, third-order nonlinear optical and free-carrier-induced effects.<sup>11</sup> Although the applied configuration is not phase-matched the detected THz field amplitudes are already surprisingly large: In a comparative experiment, using an above band gap photocarrier-based InGaAs surface-emitter<sup>12</sup> in the same set-up, generating equally high near-field amplitudes at the InGaAs surface required a two orders of magnitude higher excitation power in comparison to the PA SWG internal excitation power.

Frequency-domain data calculated from the time-domain data of Fig. 2 using Fourier transformation are plotted in Fig. 3(a). All spectra exhibit a similar shape with an amplitude maximum at 0.05 THz and a continuous amplitude drop-off into a noise floor for increasing frequency. The reference signal amplitudes measured at the SWG are above the noise level for  $f < 0.22$  THz. At  $f = 0.22$  THz and 3 mW excitation power the relative enhancement in generated THz amplitude (power) scales to an impressive factor of  $1.53 \times 10^2$  ( $2.3 \times 10^4$ ,  $I_{\text{THz}} \propto E_{\text{THz}}^2$ ) as marked by the arrow in Fig. 3(a). At 11 mW excitation power this amplitude (power) enhancement is reduced to 67 ( $4.5 \times 10^3$ ). The corresponding power-dependency of the field amplitudes generated at the PA activated waveguide is plotted in Fig. 3(b) for several

frequencies in the range of  $f = 0.05 - 0.7$  THz. For  $f > 0.3$  THz a linear relation between the THz field amplitude and excitation power is observed as it is expected for a second-order nonlinear process of DFG. This result confirms that photogenerated current surge can be ruled out as a dominating origin for THz generation: In a photoconductive THz generation process the generated field amplitude  $E_{\text{THz}}$  scales linearly with the number of photogenerated charge-carriers,<sup>13</sup> however, for subbandgap excitation the dominating absorption process within the reference and the PA silicon waveguide is two-photon absorption (TPA) and the number of TPA-generated charge carriers, increases  $\propto I_{\text{pump}}^2$ .<sup>14</sup> A deviation from a linear THz amplitude/optical pump power-dependency is observed for the generated quasi-dc field amplitude at  $f = 0.05$  THz which follows roughly a parabolic function including a positive linear and a negative quadratic term. The latter might be an indication for carrier-based screening of a PA-induced surface field.

In this work, it was demonstrated that a technically relevant amount of second-order nonlinear activity can be induced in silicon nanophotonic components by chemical surface treatment in reactive HBr-plasma. In comparison to silicon organic hybrid approaches chemical surface activation provides the important advantage of a radically simplified and CMOS-compatible fabrication process. The presented approach implies an important breakthrough for the realization of silicon waveguides with locally limited electro-optic activity, which would be difficult to fabricate with hybrid methods. Consecutive waveguide sections with and without electro-optic activity can be realized with virtually no shifts of the effective mode index. Ongoing work is directed to the application of PA silicon nanowires in electro-optic modulators.

This work was supported by the Deutsche Forschungsgemeinschaft (DFG) in frame of the “THz nanophotonics” project (Contract Nos. NA762/2-1 and KU540/50-1).

<sup>1</sup>T. W. Baehr-Jones and M. J. Hochberg, *J. Phys. Chem. C* **112**, 8085 (2008).

<sup>2</sup>J.-M. Brosi, C. Koos, L. C. Andreani, M. Waldow, J. Leuthold, and W. Freude, *Opt. Express* **16**, 4177 (2008).

<sup>3</sup>G. Lüpke, D. J. Bottomley, and H. M. van Driel, *J. Opt. Soc. Am. B* **11**, 33 (1994).

<sup>4</sup>Z. Chen, J. Zhao, Y. Zhang, J. Gang, L. Xiuhuan, R. Ce, W. Wenqing, S. Jianbo, C. Kun, W. Shuang, and S. Bao, *Appl. Phys. Lett.* **92**, 251111 (2008).

<sup>5</sup>O. A. Aktsipetrov, A. A. Fedyanin, E. D. Mishina, A. N. Rubtsov, C. W. van Hasselt, M. A. C. Devillers, and Th. Rasing, *Phys. Rev. B* **54**, 1825 (1996).

<sup>6</sup>R. S. Jacobsen, K. N. Andersen, P. I. Borel, J. Fage-Pedersen, L. H. Frandsen, O. Hansen, M. Kristensen, A. V. Lavrinenko, G. Moulin, H. Ou, C. Peucheret, B. Zsigri, and A. Bjarklev, *Nature (London)* **441**, 199 (2006).

<sup>7</sup>C. Schriever, C. Bohley, and R. B. Wehrspohn, *Opt. Lett.* **35**, 273 (2010).

<sup>8</sup>J. J. H. Gielis, P. M. Gevers, I. M. P. Aarts, M. C. M. van de Sanden, and W. M. M. Kessels, *J. Vac. Sci. Technol. A* **26**, 1519 (2008).

<sup>9</sup>M. Wächter, M. Nagel, and H. Kurz, *Appl. Phys. Lett.* **95**, 041112 (2009).

<sup>10</sup>G. W. Rieger, K. S. Virk, and J. F. Young, *Appl. Phys. Lett.* **84**, 900 (2004).

<sup>11</sup>X. Chen, N. C. Panouiu, I. Hsieh, J. I. Dadap, and R. M. Osgood, Jr., *IEEE Photon. Technol. Lett.* **18**, 2617 (2006).

<sup>12</sup>M. Suzuki, M. Tonouchi, K. I. Fujii, H. Ohtake, and T. Hirosumi, *Appl. Phys. Lett.* **89**, 091111 (2006).

<sup>13</sup>J. Shan and T. F. Heinz, *Appl. Phys. (Berlin)* **92**, 1 (2004).

<sup>14</sup>R. Dekker, N. Usechak, M. Först, and A. Driessen, *J. Phys. D: Appl. Phys.* **40**, R249 (2007).